Ultramicroscopy 111 (2011) 1037–1042

Contents lists available at ScienceDirect

Ultramicroscopy

journal homepage: www.elsevier.com/locate/ultramic

Assessment of waveguiding properties of gallium oxide nanostructures by angle resolved cathodoluminescence in a scanning electron microscope

Emilio Nogales *, Bianchi Méndez, Javier Piqueras

Departamento Física de Materiales, Universidad Complutense de Madrid 28040, Spain

ARTICLE INFO

Article history:
Received 12 May 2010
Received in revised form
3 September 2010
Accepted 9 March 2011
Available online 21 March 2011

Keywords:
Cathodoluminescence
Scanning electron microscopy
Nanowire
Waveguide

ABSTRACT

Cathodoluminescence (CL) of Ga_2O_3 nanowires and planar microstructures has been studied in a scanning electron microscope, as a function of the orientation angle of the structures relative to the position of the light detection system in the microscope chamber. CL contrast shows a marked dependence on the detection angle due to the waveguiding behaviour of the structures. The angle resolved cathodoluminescence (ARCL) measurements enable to evaluate the optical losses of guided blue-ultraviolet light in nanowires with diameters in the sub-wavelength range, deposited on graphite tape or silicon. In planar, branched feather-like microstructures, ARCL images demonstrate the directional-dependant light guiding behaviour of the nano-branches.

1. Introduction

Monoclinic gallium oxide (β-Ga_2O_3) is a semiconductor with potential applications in optoelectronics, related to its wide band gap of 4.8 eV [1–5], and gas sensing [6–8]. Also, the high refraction index of gallium oxide, of about 1.85, makes this material suitable for light guiding [9]. In particular, Ga_2O_3 nanowires have potential application as nanoconnections or nanowaveguides in optical nanodevices. Waveguiding behaviour of Ga_2O_3 nanowires [4,10] and nanowires of other crystalline oxides such as GeO_2 [11], In_2O_3 [12], ZnO [13] or SnO_2 [14] has been previously reported. For these waveguide investigations, normally an external laser beam is used as excitation source of nanowire, and the propagation of the excitation light or of the induced luminescence is studied. However, a high spatial resolution optical technique, namely CL in scanning electron microscope (SEM), which has been often used to characterize semiconductor bulk and nanostructures, has not been applied to investigate lightguide properties of nano- and microwires. In this work, CL in SEM has been used to study light propagation in gallium oxide nanowires and planar branched, feather-like, microstructures grown using a thermal evaporation–deposition technique. CL measurements as a function of orientation of the nano- or microstructures relative to the position of the light detector, hereinafter referred as angle resolved cathodoluminescence (ARCL) measurements, have been performed to investigate their light guiding properties. Data on optical losses along the wires are obtained. The application of ARCL to obtain complete information on the CL and waveguiding behaviour of complex structures, such as the Ga_2O_3 planar branched structures, is demonstrated. CL images show a marked dependence of the contrast on the detection angle. The capability of ARCL to characterize ZnO nanoscale waveguides by spectral measurements has been previously reported [15]. Also angular resolved photoluminescence has been used to study waveguide property of ZnO nanorods [16].

2. Material and methods

A disk of Ga_2O_3 compacted powder, of about 7 mm diameter, covered with metallic gallium was used as starting material. The sample was annealed under argon flow at 1150 °C for 5 h followed by a second annealing step at 1500 °C for 15 h. Since the furnace was not sealed for vacuum treatments, the annealing caused slow thermal oxidation of the metallic gallium. This process leads to the growth of Ga_2O_3 nanostructures on the pellet surface. X-ray diffraction (XRD) measurements were performed with a Philips X Pert PRO diffractometer. The morphology of the grown structures was characterised in a Leica 440 SEM. CL measurements were performed in SEM at room temperature with a Hamamatsu photomultiplier. For ARCL measurements the configuration shown in Fig. 1 was used. Both the structure, e.g. a nanowire, and CL detector are in a plane perpendicular to the electron beam direction. By rotating the nanowire, CL images for different orientations can be recorded. High resolution transmission electron

* Corresponding author. Tel.: +34 91 394 4548; fax: +34 91 394 4547.
E-mail addresses: emilio.nogales@fis.ucm.es (E. Nogales), bianchi@fis.ucm.es (B. Méndez), piqueras@fis.ucm.es (J. Piqueras).

0304-3991/$ - see front matter © 2011 Elsevier B.V. All rights reserved.
doi:10.1016/j.ultramic.2011.03.003

microscopy (HRTEM) was carried out with a field emission JEOL 3000F microscope operating at 300 kV. For HRTEM investigation the structures were detached from the pellet and dispersed in butanol. Drops of the solution with the structures were deposited on carbon coated copper microscope grids.

3. Results and discussion

The described synthesis procedure leads to the formation of β-Ga_2O_3 nanowires as well as planar microstructures with feather-like morphology. Fig. 2 shows SEM representative images of the obtained structures. The nanowires have widths between 30 and 900 nm and lengths of up to several tens of micrometres. The feather-like structures have thicknesses of few hundred nanometres, widths in the range of microns and lengths of several tens of microns. Fig. 2b shows a detail of a feather-like structure. The feather is formed by two planes that intersect along a central line. The planes contain a set of parallel steps extending from the central axis to the structure edge, which has a saw tooth-like profile. The symmetry of the structure and of the steps arrangement suggests that the central line is a twin boundary. Fig. 2c shows a detail of several nanowires. The crystalline features of the nanostructures have been studied using TEM and HRTEM. Fig. 3a shows a TEM image of a high aspect ratio nanowire of 50 nm diameter, while Fig. 3b shows the HRTEM image and the selected area electron diffraction (SAED) pattern of the nanowire. The nanowires are single crystalline and the growth direction was found to be $(-1\ 1\ 0)$. The feather-like microstructures also present a high crystal quality, as shown in the SAED pattern of Fig. 3c, corresponding to the area at the right of the central line. The zone axis is $(0\ 1\ -1)$. The different contrast observed in both halves of the feather imaged in Fig. 3b is due to the fact that they are not in the same plane so that they have different orientations relative to the electron beam.

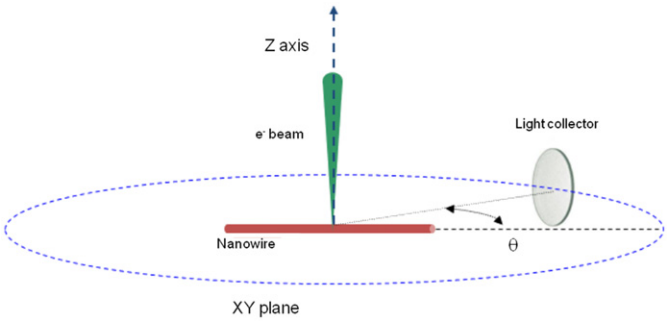

Fig. 1. Sketch of setup for ARCL measurements.

To investigate the waveguiding behaviour of the nanowires by CL, individual nanowires were removed from the pellet and placed on a graphite tape in the specimen holder of the SEM. In the 90° configuration (see Fig. 1), the light collector axis is perpendicular to the nanowire axis, and the CL image shows the luminescence emission generated in each point of the wire. On the other hand, the CL images obtained in 0°, or the equivalent 180°, configuration (light collector axis parallel to nanowire axis) show the intensity of light generated in each point after propagating along the nanowire to reach the light collector. The CL emission from the point opposite to the light collector may be affected by optical losses in its path along the nanowire, while the light generated at the position closer to the detector would be detected without losses. The CL image obtained under these conditions provides information on the possible optical losses and hence on the waveguiding properties of the nanowire. If the 0° and the 90° ARCL images are similar, negligible losses take place in the nanowire. Fig. 4a shows the SEM secondary electron (SE) image of a nanowire while Fig. 4b and c show the ARCL images recorded with the nanowire axis oriented perpendicular and parallel to the detector axis, respectively. Fig. 4b (90° orientation) shows a rather homogeneous CL intensity as expected for homogeneous nanowires. Fig. 4c corresponds to 0° orientation. It is observed that the CL intensity shows a non-uniform profile with the highest intensity in the right part, closer to the

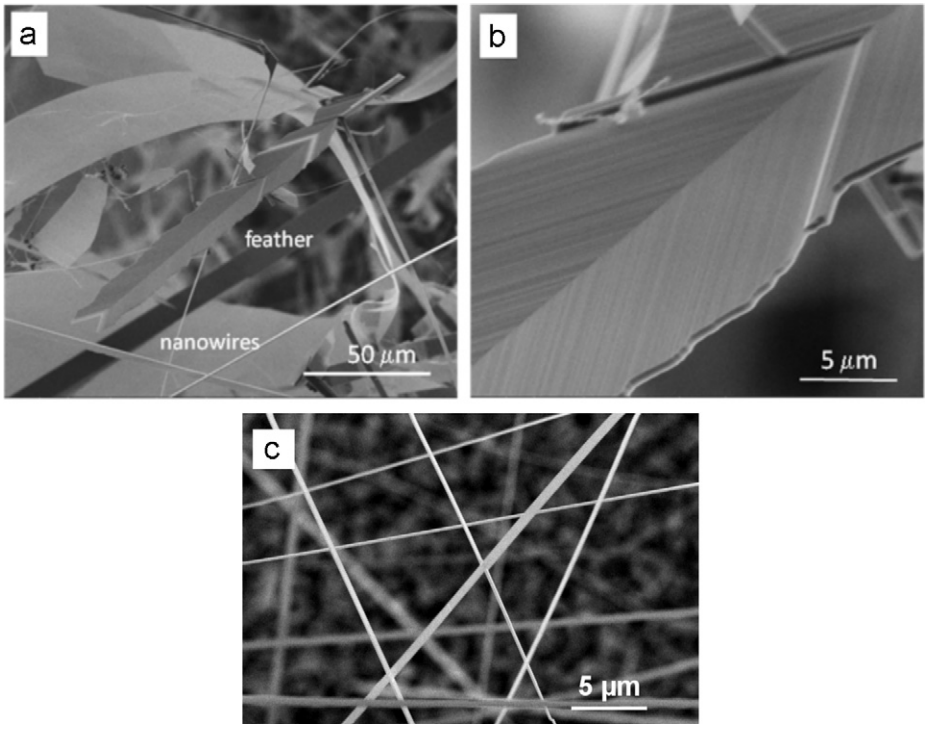

Fig. 2. SEM images of (a) a feather-like microstructure and nanowires, (b) detail of the feather showing the central line where two planes intersect and the parallel steps that form each plane and (c) nanowires with thicknesses in the range of a few hundred nanometre.

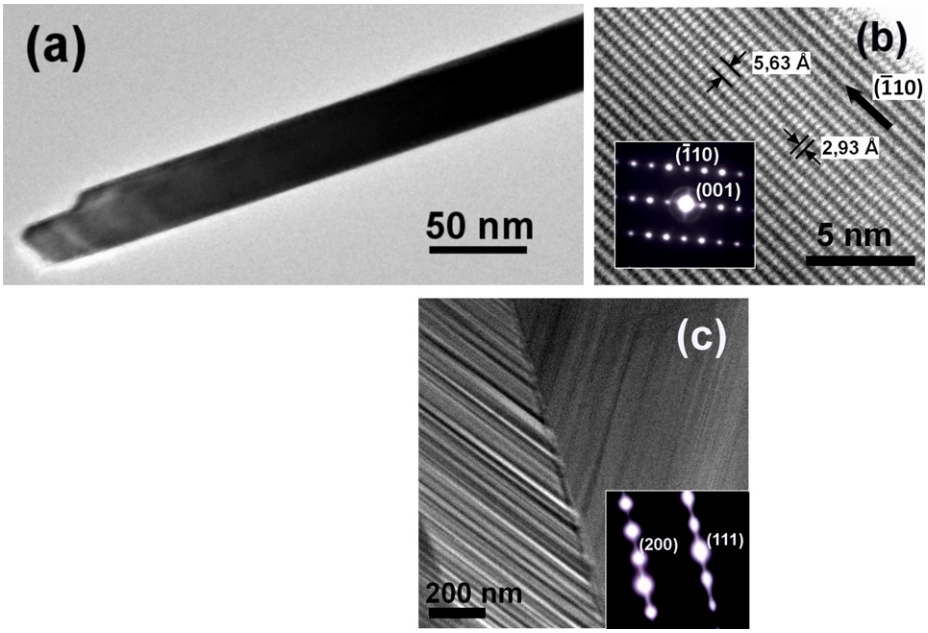

Fig. 3. (a) TEM image of a nanowire of about 50 nm thickness. (b) HRTEM and SAED pattern of the nanowire shown in (a), showing that the growth direction ($-1\ 1\ 0$). (c) TEM image of a feather-like structure, which shows the central twin boundary and the contrast associated to the steps observed in Fig. 2(b). Inset: SAED pattern of the right part of the feather, showing that the zone axis is ($0\ 1\ -1$).

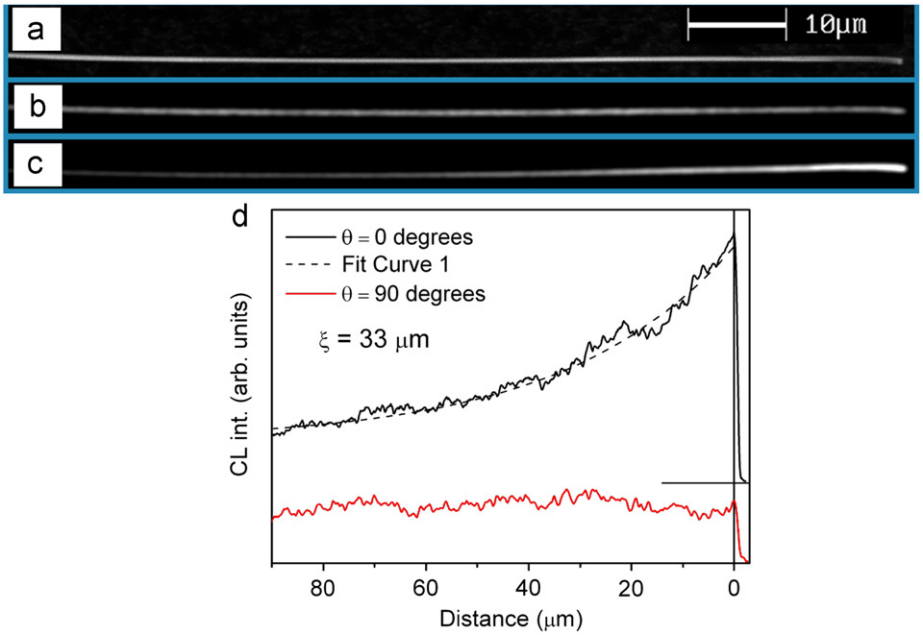

Fig. 4. (a) SE image of nanowire on graphite tape with cross-sectional dimension of about 450 nm and a length of 90 µm. (b) ARCL image recorded at 90° configuration, corresponding to the wire axis perpendicular to the light collector axis. (c) ARCL image recorded at 0° configuration, corresponding to the wire axis placed along the light collector axis. (d) ARCL intensity profiles along the wire for the 0° (upper, solid black line) and 90° (lower, solid red line) configurations. An exponential fit to the upper curve is also plotted (upper dashed, black line), yielding a decay length for the optical losses of $\xi = 33$ µm. (For interpretation of the references to color in this figure legend, the reader is referred to the web version of this article.)

detector, revealing the existence of optical losses as the luminescence emission travels along the wire. After a 180° rotation of the wire, the brighter end of the wire becomes darker (not shown), which confirms that optical losses determine the intensity distribution in Fig. 4c. Optical losses along a medium can be quantified by an exponential law, $I = I_0 \exp(-x/\xi)$, being ξ the decay length. Fig. 4d shows the CL intensity profiles along the nanowire for $\theta = 90°$ (lower, red solid line) and 0° (upper, black solid line), extracted from the ARCL images of Fig. 4b and c, respectively. The lower curve shows a rather uniform emission intensity profile while the upper curve follows a decay profile, which fits to the exponential law (upper, black dashed line) with $\xi = 33$ µm. The results shown in Fig. 4 is representative for the wires on this substrate and demonstrate the application of ARCL for quantitative assessment of waveguiding of nanowires. The obtained ξ value represents a strong decay as compared with those reported on SnO_2 [14] or Ga_2O_3 [17]

nanowires. The calculation of the losses of the nanostructures on graphite tape, taking into account the exponential decay obtained from Fig. 4, gives a value of the order of 100 dB/mm. This is much higher than the value obtained for a free standing Ga_2O_3 nanowire in the work by Wang et al. [17]. Indeed, the high refractive index of gallium oxide [9], the good crystal quality and the very smooth surfaces of the nanowires in our work (see Fig. 2c and Fig. 3a) should result in good waveguiding behaviour. Therefore, the origin of strong losses may be related to effects in the nanowire-substrate interface. In order to study this possibility, some nanowires were deposited on silicon substrate wafers. Fig. 5a shows the SE image of a nanowire of 250 nm diameter and 70 μm length on a Si substrate. This nanowire is a representative case of lateral dimensions in the sub-wavelength range for visible light propagation. The corresponding ARCL images for $\theta=90^\circ$ and $\theta=0^\circ$ are shown in Fig. 5b and c, respectively. CL profiles along the wire axis are rather uniform and independent of the detection angle (Fig. 5d). The feature at around 20 μm from the right side, observed in the SE image does not avoid light propagation along the wire, as can be observed in the CL images. We have also performed attenuation measurements in longer Ga_2O_3 wires on silicon substrates. The CL intensity profiles along the wire axis, for 0° and 90° orientations, in a nanowire of 180 μm length and thickness of 750 nm, are shown in Fig. 5e. It can be appreciated that losses along nanowires on a Si substrate are negligible for the studied lengths and the profile of the ARCL signal seems to be independent on the detection angle. In fact, from the present data it is not feasible to obtain a numerical value for the losses as CL intensity for 0° configuration remains uniform along the nanowire. In the work performed by Wang et al. [17] part of the losses were attributed to surface contamination. In our case, thanks to a solution-free procedure to place the wires on the substrates, the contamination is very low, as observed in the SEM images. This can explain the very good waveguiding behaviour for the case of the Si substrate. These results indicate that the observed losses for nanowires on graphite (Fig. 4) are due to the presence of the substrate and not to internal absorption and/or surface scattering of light by the nanowires themselves and suggest the possibility to integrate these nanowires in the standard silicon based electronics. In the case of the rough, conductive graphite tape, the losses should be related to the many contacting points of the nanofibre with the substrate. Absorption and/or scattering of part of the evanescent wave by the conductive graphite can be reasonably considered to occur. The overall effect would be the strong loss that has been measured with this CL based technique. The CL and waveguiding properties that we have observed are quite independent on the nanowire diameter within the studied range.

It is to be noticed that in this work the propagation of the light generated in the wire by excitation with electron beam is investigated. Information on light generation, using cathodoluminescence, as well as on the optical losses in the wire can be obtained in a single experiment. Similar experiments were performed in CdS nanowires with laser beam excitation [18]. The room temperature CL spectrum of the nanowires (Fig. 6) shows a complex UV-blue

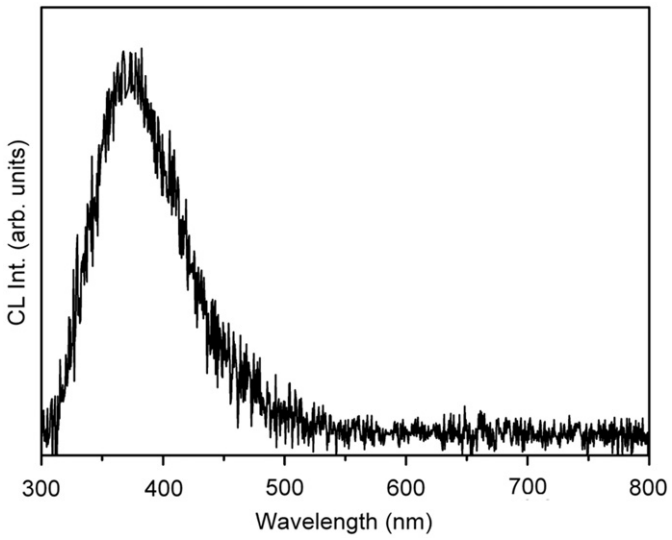

Fig. 6. CL spectrum of a nanowire, representative for the gallium oxide structures under study.

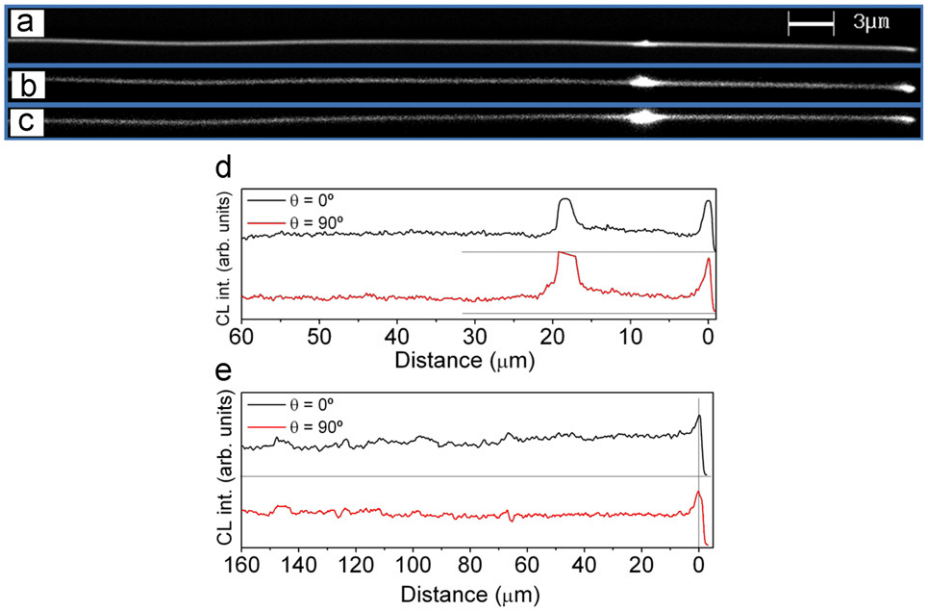

Fig. 5. (a) SE image of a nanowire with diameter of about 250 nm and length of 70 μm, on a silicon wafer. (b) ARCL image with 90° configuration. (c) ARCL image with 0° configuration. (d) ARCL intensity profiles along the wire shown in (a) for the 0° (upper, solid black line) and the 90° (lower, solid red line) configurations. (e) ARCL intensity profiles along a wire 750 nm wide and 160 μm long, for the 0° (upper, solid black line) and the 90° (lower, solid red line) configurations. (For interpretation of the references to color in this figure legend, the reader is referred to the web version of this article.)

band centred at about 360 nm (3.4 eV) related to intrinsic defects involving oxygen vacancies [1]. Hence, the present experiments refer to waveguiding in nanowires with cross-sectional dimensions comparable to the wavelength of the propagating light.

ARCL has been also used to study waveguide properties of the above described feather-like microstructures. Fig. 7a shows the SE image of one of these microstructures and Fig. 7b and c show the ARCL images at 0° and 180°, respectively, corresponding to detection in opposite ends of the feather. Clear differences can be observed between the two images. The effect of optical losses along the length of the structure, observed in the nanowires (see Fig. 4c) is also apparent in Fig. 7b, in which higher CL intensity is observed in the feather tip, closer to the detector. In the 180° configuration, Fig. 7c, these longitudinal optical losses are revealed by the higher intensity in the left part of the feather, which, in this case, is closer to the detector. Fig. 7c also shows a strong intensity increase along the branches that protrude from the edge, which act as waveguides and become efficient collection paths of the light for this detection angle. These paths are related to steps in the feather structures, as SEM images show. Comparison of Fig. 7b and c shows that light collection along the branches is directional-dependant. In order to confirm that this directional effect is also observed with external light, a similar structure has been studied with optical microscopy, as shown in Fig. 8. Fig. 8a shows the optical image of a homogeneously illuminated feather, while Fig. 8b and c show the images by illuminating only one of the ends with white light. The latter two images show that light is guided along the structure in both directions. However, in the specific points indicated by arrows, similar to the branches seen in the structure showed in Fig. 7, light is detected when light is guided from left to right (Fig. 8c), but not when guiding from right to left (Fig. 8b), confirming the directionality observed with ARCL.

This directional dependant behaviour may be of potential interest for asymmetric directional coupling in optical nanodevices. Several works have reported the fabrication of branched nanostructures with a wire that acts as a central backbone from which grow the branches [19,20] and mentioned the capabilities to be used in electronic and photonic devices in three dimensions. We show that the feather-like structures behave as two-dimensional branched structures with directional-dependant behaviour.

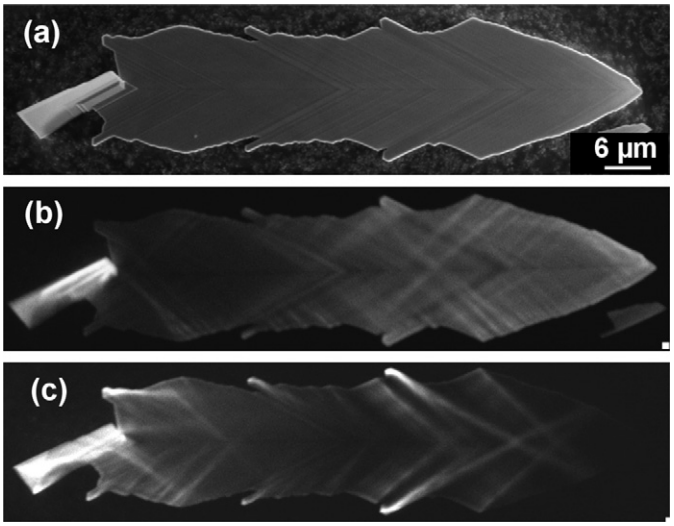

Fig. 7. (a) SE image of a feather-like structure with branches protruding from the edges. (b) ARCL image for 0° configuration (detector at the right of the structure), showing a longitudinal intensity decay similar to that observed in the nanowires (Fig. 4(c)). (c) ARCL image for 180° configuration (detector at the left of the structure), showing the longitudinal intensity decay and strong intensity along the branches, which act as waveguides. Comparison between Fig. 7(b) and 7(c) shows a strong directional-dependant light collection along the branches.

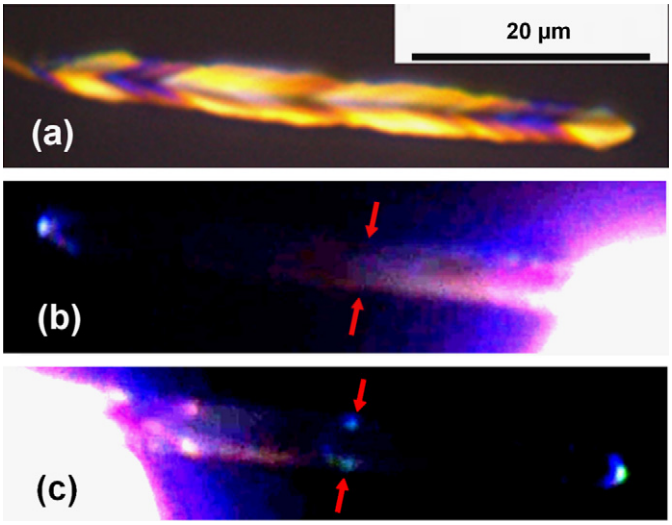

Fig. 8. Optical microscopy images of a feather-like structure illuminated (a) homogeneously, (b) at the right end and (c) at the left end. The arrows show the effect of the presence of branches on the waveguide behaviour. Light is collected at edge protruding points only when guided from left to right, demonstrating the directional-dependant effect observed for the emitted light in Fig. 7.

4. Conclusions

In conclusion, nanowires and planar, feather-like microstructures of monoclinic gallium oxide with good crystal quality have been grown by a thermal method. ARCL has been used to investigate the waveguiding behaviour of the structures. It has been demonstrated that ARCL enables the quantitative study of optical losses along the nanowires and to determine their CL emission. In particular good UV light transmission is observed in nanowires with sub-wavelength cross-sectional dimensions, placed on a silicon wafer. ARCL shows that feather-like structures present directional dependant waveguiding behaviour along their growth axis, revealing branch structures acting as directional-dependant waveguides. ARCL appears as a useful technique to investigate luminescence with high spatial resolution in materials with waveguiding behaviour, providing additional information to that obtained by conventional CL.

Acknowledgment

This work has been supported by MEC (projects MAT2006-01259, MAT2009-07882 and Consolider Ingenio CSD 2009-00013) and BSCH-UCM (Group 910146).

References

[1] L. Binet, D. Gourier, J. Phys. Chem. Solids 59 (1998) 1241.
[2] K.-W. Chang, J.-J. Wu, Adv. Mater. 16 (2004) 545.
[3] E. Nogales, B. Méndez, J. Piqueras, Appl. Phys. Lett. 86 (2005) 113112.
[4] E. Nogales, J.A. García, B. Méndez, J. Piqueras, Appl. Phys. Lett. 91 (2007) 133108.
[5] D.P. Yu, J.L. Bubendorff, J.F. Zhou, Y. Leprince-Wang, M. Troyon, Solid State Commun. 124 (2002) 417.
[6] S.I. Maximenko, L. Mazeina, Y.N. Picard, J.A. Freitas Jr., V.M. Bermudez, S.M. Prokes, Nano Lett. 9 (2009) 3245.
[7] M. Fleischer, J. Giber, H. Meixner, Appl. Phys. A 54 (1992) 560.

[8] C. Baban, Y. Toyoda, M. Ogita, Thin Solid Films 484 (2005) 369.
[9] M. Passlack, E.F. Schubert, W.S. Hobson, M. Hong, N. Moriya, S.N.G. Chu, K. Konstandinidis, J.P. Mannaerts, M.L. Schnoes, G.J. Zydzik, J. Appl. Phys. 77 (1995) 686.
[10] E. Nogales, B. Méndez, J. Piqueras, J.A. García, Nanotechnology 20 (2009) 115201.
[11] P. Hidalgo, B. Méndez, J. Piqueras, Nanotechnology 18 (2007) 155203.
[12] T. Tsuruoka, C.H. Liang, K. Teraba, T. Hasegawa, J. Opt. A: Pure Appl. Opt. 10 (2008) 055201.
[13] T. Voss, G.T. Svacha, E. Mazur, S. Müller, C. Ronning, D. Konjhodzic, F. Marlow, Nano Lett. 7 (2007) 3675.
[14] M. Law, D.J. Sirbuly, J.C. Johnson, J. Goldberger, R.J. Saykally, P. Yang, Science 305 (2004) 1269.
[15] C. Li, M. Gao, C. Ding, X. Zhang, L. Zhang, Q. Chen, L.M. Peng, Nanotechnology 20 (2009) 175703.
[16] W. Li, M. Gao, R. Cheng, X. Zhang, S. Xie, L.M. Peng, Appl. Phys. Lett. 93 (2008) 023117.
[17] Fei Wang, Zhanghua Han, Limin Tong, Physica E 30 (2005) 150.
[18] C.J. Barrelet, A.B. Greytak, C.M. Lieber, Nano Lett. 4 (2004) 1981.
[19] K.A. Dick, K. Deppert, M.W. Larsson, T. Martensson, W. Seifert, W.R. Wallenberg, L. Samuelson, Nat. Mater. 3 (2004) 380.
[20] Y. Jung, D.-K. Ko, R. Agarwal, Nano Lett. 7 (2007) 264.